Available online at www.sciencedirect.com

ScienceDirect

Mendeleev Commun., 2019, **29**, 22–24

Mendeleev Communications

Trimetallic NiCoM catalysts (M = Mn, Fe, Cu) for methane conversion into synthesis gas

Igor V. Zagaynov,*[a] Alexey S. Loktev,[b,c] Igor E. Mukhin,[b] Anatoly A. Konovalov,[a] Alexey G. Dedov[b,c] and Ilya I. Moiseev[b,c]

[a] *A. A. Baikov Institute of Metallurgy and Materials Science, Russian Academy of Sciences, 119334 Moscow, Russian Federation. E-mail: igorscience@gmail.com*
[b] *I. M. Gubkin Russian State University of Oil and Gas, 119991 Moscow, Russian Federation*
[c] *N. S. Kurnakov Institute of General and Inorganic Chemistry, Russian Academy of Sciences, 119991 Moscow, Russian Federation*

DOI: 10.1016/j.mencom.2019.01.006

The investigation of dry reforming of methane (DRM) and the partial oxidation of methane (POM) over mesoporous catalysts containing trimetallic active component NiCoM (M = Mn, Fe, or Cu) supported on ceria solid solution has demonstrated that the introduction of 10 mol% Mn can enhance the stability of a NiCo active component (anticoking performance) due to a smaller metal particle size, alloy formation, and a synergetic effect between Ni–Co–Mn.

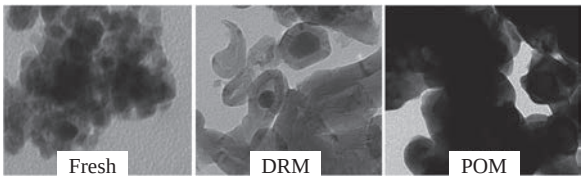

The conversion of methane into valuable products,[1,2] including synthesis gas as a key intermediate,[3] is of considerable importance. The dry reforming of methane (DRM) is promising for biogas utilization, conversion of greenhouse gases into valuable chemicals, and a reduction of carbon dioxide emissions.[4,5] Since the steam reforming of methane (SRM) and DRM are endothermic and, hence, energy-intensive, the partial oxidation of methane (POM) has some advantages: the composition of synthesis gas is preferable for its processing into methanol, the Fischer–Tropsch synthesis of liquid hydrocarbons, and the cost of production is lower than that of SRM due to exothermic reaction. Thus, POM and DRM are promising and environmentally benign cost-effective processes.

DRM and POM studies have been oriented to the development of catalysts with good lifetime stability. Noble metals work very well with minimum carbon deposition, but they are expensive. Nickel is suitable for replacing noble metals,[6] but this catalyst can be deactivated due to coking. A promising strategy is the doping of Ni to modify the active component and to form a bimetallic system. Noble metals (Pt, Pd, Rh, Ru, Ir, Au, and Ag) can promote the reducibility of nickel and, thus, increase the number of active sites. However, despite the excellent catalytic properties, using noble metals is limited due to the high price and low availability of noble metals.[7] Transition metals (Co, Fe, and Cu) have also been added to Ni-based catalysts to create bimetallic systems, and the NiCo bimetallic catalyst was the best[8–10] because Co can slow down the reduction of Ni and stabilize the catalyst, resulting in a small size of metal particles. Moreover, Co sites have lower energy barriers for methane activation on the NiCo surface[6,11] because methane decomposition is the most difficult step. It was shown that the activity is closely related to the Ni/Co ratio, and the molar ratio 80Ni/20Co is optimal.[12,13] Generally, the carbon formation is efficiently hindered by the formation of NiCo alloy during the catalytic test as compared to the single Ni active sites.[14] However, catalyst deactivation remains a serious problem. To enhance the stability of the catalyst, the addition of a third metal (M) can be proposed. For this purpose, iridium promoter was used to improve the reduction of the catalyst, and CH_4 and CO_2 conversions were increased over 20%;[15] however, it is expensive.

Therefore, this work was focused on the development of stable noble metal-free catalysts based on polymetallic active components NiCoM, where M is Mn, Fe, or Cu, immobilized on ceria solid solution support $Gd_{0.1}Ti_{0.1}Zr_{0.1}Ce_{0.7}O_2$ for DRM and POM processes.

Table 1 shows the main characteristic of fresh catalysts with a mesoporous structure. Samples have type IV isotherms and H2 hysteresis loops (not shown). The range of pore sizes is narrow (2–15 nm). The oxide support had an initial surface area of 83 $m^2\ g^{-1}$.[16] This value is lower than that of synthesized catalysts, so the structural modification occurs during combined

Table 1 Characteristics of fresh catalysts.

Sample	Composition	d_{XRD}/nm (support)	S_{BET}/ $m^2\ g^{-1}$	D_{pore}/nm
20Mn	5 wt% NiCoMn–$Gd_{0.1}Ti_{0.1}Zr_{0.1}Ce_{0.7}O_2$ (Ni/Co/Mn = 64/16/20 mol)	10	81	2–15
10Mn	5 wt% NiCoMn–$Gd_{0.1}Ti_{0.1}Zr_{0.1}Ce_{0.7}O_2$ (Ni/Co/Mn = 72/18/10 mol)	7	88	2–15
20Fe	5 wt% NiCoFe–$Gd_{0.1}Ti_{0.1}Zr_{0.1}Ce_{0.7}O_2$ (Ni/Co/Fe = 64/16/20 mol)	8	94	2–10
10Fe	5 wt% NiCoFe–$Gd_{0.1}Ti_{0.1}Zr_{0.1}Ce_{0.7}O_2$ (Ni/Co/Fe = 72/18/10 mol)	7	95	2–10
20Cu	5 wt% NiCoCu–$Gd_{0.1}Ti_{0.1}Zr_{0.1}Ce_{0.7}O_2$ (Ni/Co/Cu = 64/16/20 mol)	7	94	2–8
10Cu	5 wt% NiCoCu–$Gd_{0.1}Ti_{0.1}Zr_{0.1}Ce_{0.7}O_2$ (Ni/Co/Cu = 72/18/10 mol)	9	85	2–15

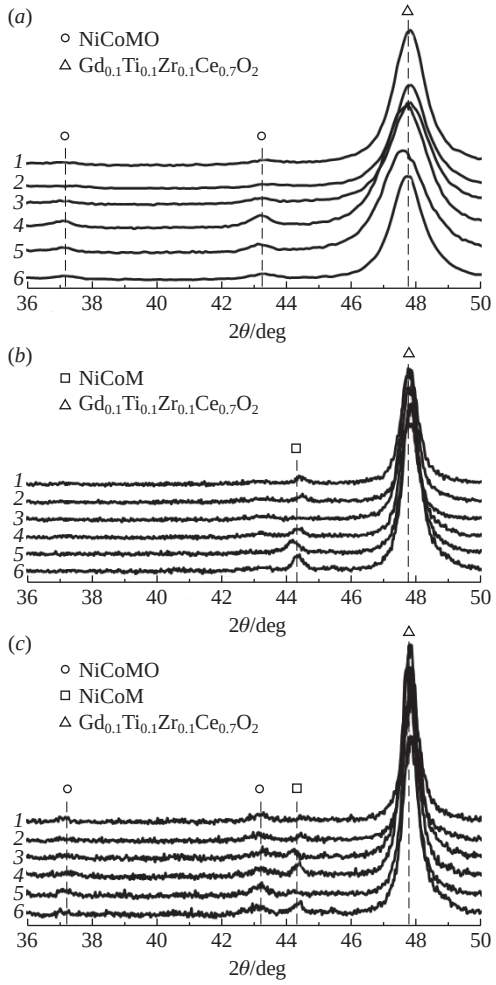

Figure 1 XRD patterns of (*a*) fresh catalysts and catalysts used after (*b*) DRM and (*c*) POM: (*1*) 20Mn, (*2*) 10Mn, (*3*) 20Fe, (*4*) 10Fe, (*5*) 20Cu, and (*6*) 10Cu.

co-precipitation, and an active oxide component provides a small increase in surface area, whereas other methods can only decrease the surface due to pore blockage by active component. The BET surface and BJH pore size distribution are given in Table 1.

The XRD analysis of fresh catalysts [Figure 1(*a*)] indicates that support is correctly synthesized with the active component. A shift of the diffraction peak of the support, compared to pure ceria, was observed[12,16] due to solid solution formation. The average crystallite size of the support was estimated at 8–10 nm using the Scherrer equation and confirmed by TEM images [Figure 2(*a*)]. The diffraction peaks of a cubic (NiCoM)O phase were observed between the diffraction peaks of cubic (*Fm*3*m*) NiO and CoO phases. Thus, the formation of two solid solution phases based on CeO_2 and NiO was detected, and the formation of other phases (carbides, Ni–Co–O spinel, *etc*.) was not observed.

The activity of the catalysts and product selectivity (CO and H_2) increased with the reaction temperature (Table S1) and reached maximum values at 950 °C; a further increase (> 1000 °C) led to a decrease in these parameters. The conversion and yield were better for systems with the addition of Mn, but the parameters were close at 950 °C, leveling out the effect of the third component. The best sample was 10Mn (*i.e*., the system with the active component 72Ni18Co10Mn). As the content of the third component was increased from 10 to 20 mol%, the activity somewhat diminished, apparently, due to a decrease in the proportion of the most active Ni. The H_2/CO ratio in the produced syngas was 1 : 1 for DRM or 2 : 1 for POM at these temperatures. The catalyst 10Mn (72Ni18Co10Mn) is more active than the system 80Ni20Co[13] and industrial catalysts like Katalco 57–4 (16% Ni/Al_2O_3).[17] The long-term stability of the synthesized catalysts was tested (Figure S1, the catalyst 10Mn in POM as an example). The developed catalyst was stable in time, and an oscillatory process occurred with the formation of carbon (a decrease in the yield of CO and H_2) and its oxidation (an increase in the yield of CO and H_2).

The XRD patterns of the catalysts after DRM [Figure 1(*b*)] and POM [Figure 1(*c*)] indicate that the diffraction peaks of a (NiCoM)O phase are still present after POM but not after DRM. NiCoM alloy formation was detected in both processes, and it was the only phase after DRM. The formation of other phases (carbides, spinel, perovskite, *etc*.) was not observed. The formation of a cubic solid solution (support) and cubic secondary phases of (NiCoM)O or NiCoM was confirmed by SAED (Figure 2, insert), and electron diffraction confirmed the formation of a graphite-like structure after DRM.

Changes in the particle size and some information on coking (the system 10Mn as an example) are shown in TEM images (decoration/encapsulation of Ni based nanoparticles can be present simultaneously[18]). The average particle sizes of the fresh and used catalysts are about 10 and 20–35 nm, respectively. Coke formation was clearly observed in DRM in the form of amorphous carbon and carbon nanotubes. According to SEM data, the surface after POM was almost clean [had amorphous carbon, which cannot be detected by SEM, Figure S2(*b*),(*d*)], while carbon nanotubes were formed in the DRM process [Figure S2(*a*),(*c*)]. The coking is more intense in systems with 20 mol% additives, especially, in Fe-doped catalysts.

The coke accumulated in the catalysts is the result of two processes: coking ($CH_4 \rightarrow C + 2H_2$; $2CO \rightarrow C + O_2$; $CO + H_2 \rightarrow$ $\rightarrow C + H_2O$) and carbon gasification (through inverse of the indicated reactions). The amount of carbon deposited on the used catalyst was estimated by TG-DSC (this parameter depends on the relative rate of the processes). The system 10Mn after POM has two characteristic mass loss peaks [Figure S3(*a*)] and a corresponding carbon oxidation exothermic effect: at 300–350 °C,

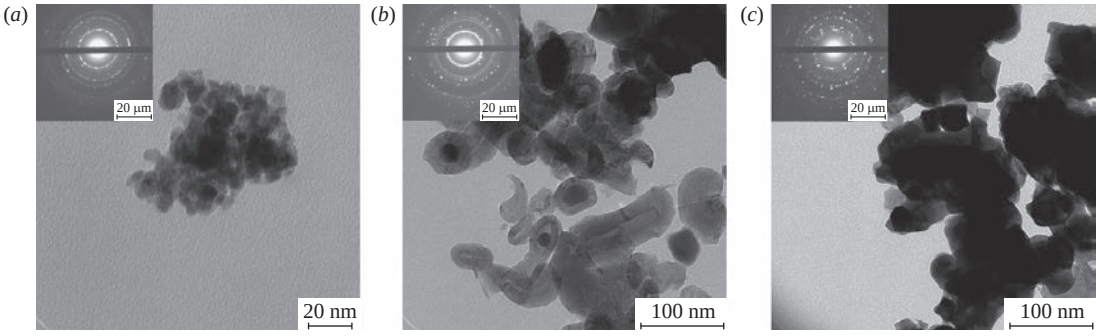

Figure 2 TEM images of (*a*) fresh catalyst and catalysts used after (*b*) DRM and (*c*) POM (sample 10Mn).

a slight change in mass is associated with the oxidation of amorphous carbon, and at 500–600 °C (6%), the formation of carbon corresponds to 1.5 $mg_C\ g^{-1}_{cat}\ h^{-1}$. The system 10Mn after DRM [Figure S3(*b*)] has only one characteristic mass loss peak, which is associated with the oxidation of multi-walled carbon nanotubes (500–600 °C), and the formation of carbon corresponds to 0.6 $mg_C\ g^{-1}{}_{cat}\ h^{-1}$. The trimetallic catalysts showed a small quantity of deposited carbon. The monometallic Ni catalyst had a larger amount of deposited carbon than the bi- and trimetallic catalysts.[19] The inhibition of carbon deposition by trimetallic NiCoMn can originate from kinetic control on the metal surface at the steady-state process because the amount of carbon deposited ($mg_C\ g^{-1}_{cat}\ h^{-1}$) decreased with the stream time.

Thus, the DRM and POM were carried out over ceria-based solid solution supported trimetallic catalysts, which were prepared by co-precipitation. The results show that the introduction of 10 mol% Mn can enhance the activity and stability of NiCo bimetallic catalysts demonstrated earlier. Compared with monometallic and bimetallic catalysts, the developed systems exhibited not only higher activity but also better stability and carbon resistance. In our case, higher carbon resistance was due to the formation of a solid solution of the support based on ceria-doped system, and the solid solution of active component (synergic effect between three metals), and strong metal-support interaction. In addition, the trimetallic catalyst showed the negligible amount of deposited carbon due to balancing the reactions of oxidative [CO_2 (O_2), H_2O] and reductive (CH_4, CO, H_2) species on the catalyst surface.[20] The catalyst 10Mn can be recommended for use in the DRM and POM processes at a temperature of 850 °C.

This study was supported by the Russian Science Foundation (grant no. 17-73-10331, development of polymetallic catalysts, surface investigation, TG, TEM, and grant no. 14-13-01007, catalytic tests), grant of the Ministry of Education and Science of the Russian Federation within realization of the state task 4.6718.2017/6.7 (the leading researchers on a constant basis, XRD and SEM analysis).

Online Supplementary Materials

Supplementary data associated with this article can be found in the online version at doi: 10.1016/j.mencom.2019.01.006.

References

1 Y. Kathiraser, U. Oemar, E. T. Saw, Z. Li and S. Kawi, *Chem. Eng. J.*, 2015, **278**, 62.
2 R. Horn and R. Schlögl, *Catal. Lett.*, 2015, **145**, 23.
3 J. Rostrup-Nielsen and L. J. Christiansen, *Concepts in Syngas Manufacture*, Imperial College Press, London, 2011.
4 M. Usman, W. M. A. Wan Daud and H. F. Abbas, *Renewable Sustainable Energy Rev.*, 2015, **45**, 710.
5 Y. Wang, L. Yao, S. Wang, D. Mao and C. Hu, *Fuel Process. Technol.*, 2018, **169**, 199.
6 Z. Liu, P. Lustemberg, R. A. Gutiérrez, J. J. Carey, R. M. Palomino, M. Vorokhta, D. C. Grinter, P. J. Ramírez, V. Matolín, M. Nolan, M. V. Ganduglia-Pirovano, S. D. Senanayake and J. A. Rodriguez, *Angew. Chem. Int. Ed.*, 2017, **56**, 13041.
7 Z. Bian, S. Das, M. H. Wai, P. Hongmanorom and S. Kawi, *ChemPhysChem*, 2017, **18**, 3117.
8 M. Sharifi, M. Haghighi, F. Rahmani and S. Karimipour, *J. Nat. Gas Sci. Eng.*, 2014, **21**, 993.
9 J. Zhang, H. Wang and A. K. Dalai, *J. Catal.*, 2017, **249**, 300.
10 T. Odedairo, J. Ma, J. Chen, S. Wang and Z. Zhu, *J. Solid State Chem.*, 2016, **233**, 166.
11 E. D. German and M. Sheintuch, *J. Phys. Chem. C*, 2013, **117**, 22811.
12 I. V. Zagaynov, A. S. Loktev, A. L. Arashanova, V. K. Ivanov, A. G. Dedov and I. I. Moiseev, *Chem. Eng. J.*, 2016, **290**, 193.
13 I. V. Zagaynov, A. S. Loktev, I. E. Mukhin, A. G. Dedov and I. I. Moiseev, *Mendeleev Commun.*, 2017, **27**, 509.
14 B. Abdullah, N. A. Abd Ghani and D.-V. N. Vo, *J. Cleaner Prod.*, 2017, **162**, 170.
15 A. H. Fakeeha, A. A. Ibrahim, Y. Arafat, H. Atia, A. E. Abasaeed and A. S. Al-Fatesh, *Can. J. Chem. Eng.*, 2018, **96**, 955.
16 I. V. Zagaynov, *Ceram. Int.*, 2015, **41**, 8730.
17 A. L. Lapidus, F. G. Zhagfarov, A. B. Yelkin and C. Zyong, *Tekhnologii Nefti i Gaza*, 2010, no. 4, 15 (in Russian).
18 M. Li and A. C. van Veen, *Appl. Catal., B*, 2018, **237**, 641.
19 B. AlSabban, L. Falivene, S. M. Kozlov, A. Aguilar-Tapia, S. Ould-Chikh, J.-L. Hazemann, L. Cavallo, J.-M. Basset and K. Takanabe, *Appl. Catal., B*, 2017, **213**, 177.
20 F. Wang, L. Xu, W. Shi, J. Zhang, K. Wu, Y. Zhao, H. Li, H. X. Li, G. Q. Xu and W. Chen, *Nano Res.*, 2017, **10**, 364.

Received: 6th August 2018; Com. 18/5661